Discontinuous low-velocity zones in southern Tibet question the viability of the channel flow model

GYÖRGY HETÉNYI[1,2]*, JÉRÔME VERGNE[2,3], LAURENT BOLLINGER[4] & RODOLPHE CATTIN[2,5]

[1]*Department of Earth Sciences, ETH Zürich, Zürich, Switzerland*

[2]*Laboratoire de Géologie, Ecole Normale Supérieure – CNRS UMR8538, Paris, France*

[3]*Ecole et Observatoire des Sciences de la Terre, Strasbourg, France*

[4]*Laboratoire de Détection et de Géophysique, CEA, Bruyères-le-Châtel, France*

[5]*Laboratoire Géosciences Montpellier, Université Montpellier 2, Montpellier, France*

**Corresponding author (e-mail: gyorgy.hetenyi@erdw.ethz.ch)*

Abstract: Low-velocity zones ('bright spots') imaged by the INDEPTH seismic experiment in southern Tibet are extensively interpreted as widespread partial melt within the crust, which has given a strong support for the channel flow model. These suggest that a continuous seismic low-velocity zone underlies Tibet on the large scale. Here we take advantage of the Hi-CLIMB seismic experiment which includes a dense south–north profile and a lateral 2D seismic network to assess the vertical and the horizontal extension of low-velocity zones in southern Tibet. Several approaches including migration, amplitude analysis and waveform inversion of receiver functions are performed to detect crustal low-velocity zones using this new seismological dataset. Our results reveal localized and discontinuous low-velocity zones in Tibet. They indicate that the vertical extension of the low-velocity zones is about 10 km, and their maximum horizontal length appears to be *c*. 50 km. Our study suggests a partial correlation between the location of these low-velocity zones and the spatial distribution of Tibetan grabens. These results, especially the non-continuity of low-velocity zones, together with the observed regular value of mean crustal V_P/V_S ratio, question the existence of widespread partial melt of the southern Tibetan crust and, therefore, the viability of the channel flow model.

The Tibetan Plateau and the Himalayas are the results of the well-known ongoing convergence between the Indian and Eurasian plates (e.g. Molnar *et al.* 1973; Molnar & Tapponnier 1975; Patriat & Achache 1984; Molnar & Stock 2009). However, the accommodation of this convergence, especially the localization of the deformation within the Tibetan Plateau is still a matter of debate. Two end-member models are commonly proposed. On the one hand most of the deformation occurs along the active faults that bound the major rigid Tibetan blocks (e.g. Avouac & Tapponnier 1993). On the other hand the convergence rate is mostly accommodated by internal deformation within the blocks related to the viscous behaviour of the continental lithosphere (e.g. Houseman & England 1993; England & Molnar 1997). Global Positioning System measurements are key data to discuss these two models. However, as previously mentioned by Thatcher (2007), due to the non-homogeneous GPS data coverage (e.g. Zhang *et al.* 2004), the distinction between block and continuum models depends upon the scale of the study area. A complementary approach is the use of heat flow data to constrain the rheological behaviour of the crust according to its thermal structure. These measurements give a high Tibetan heat flow (between 61–319 mW m^{-2} in southern Tibet), which favours viscous behaviour and thus may support the continuum model. However, heat flow data are only available at a few locations on the plateau (Fig. 1), and only a few of them are considered to be of good quality (e.g. Pollack *et al.* 1993; Fig. 1). Thus the analysis of heat flow gives only spatially limited constraints on the rheological behaviour of the Tibetan crust.

A major contribution to our knowledge of the physical properties of the plateau in southern Tibet comes from the passive and active seismological experiments, like the INDEPTH projects (International Deep Profiling of Tibet and the Himalayas; Zhao *et al.* 1993; Nelson *et al.* 1996; Haines *et al.* 2003). Active seismic surveys conducted during INDEPTH II in the Yadong-Gulu rift (Fig. 1) show unusually large negative amplitudes in near vertical reflections (i.e. larger than 10 dB above

From: GLOAGUEN, R. & RATSCHBACHER, L. (eds) *Growth and Collapse of the Tibetan Plateau.* Geological Society, London, Special Publications, **353**, 99–108.
DOI: 10.1144/SP353.6 0305-8719/11/$15.00

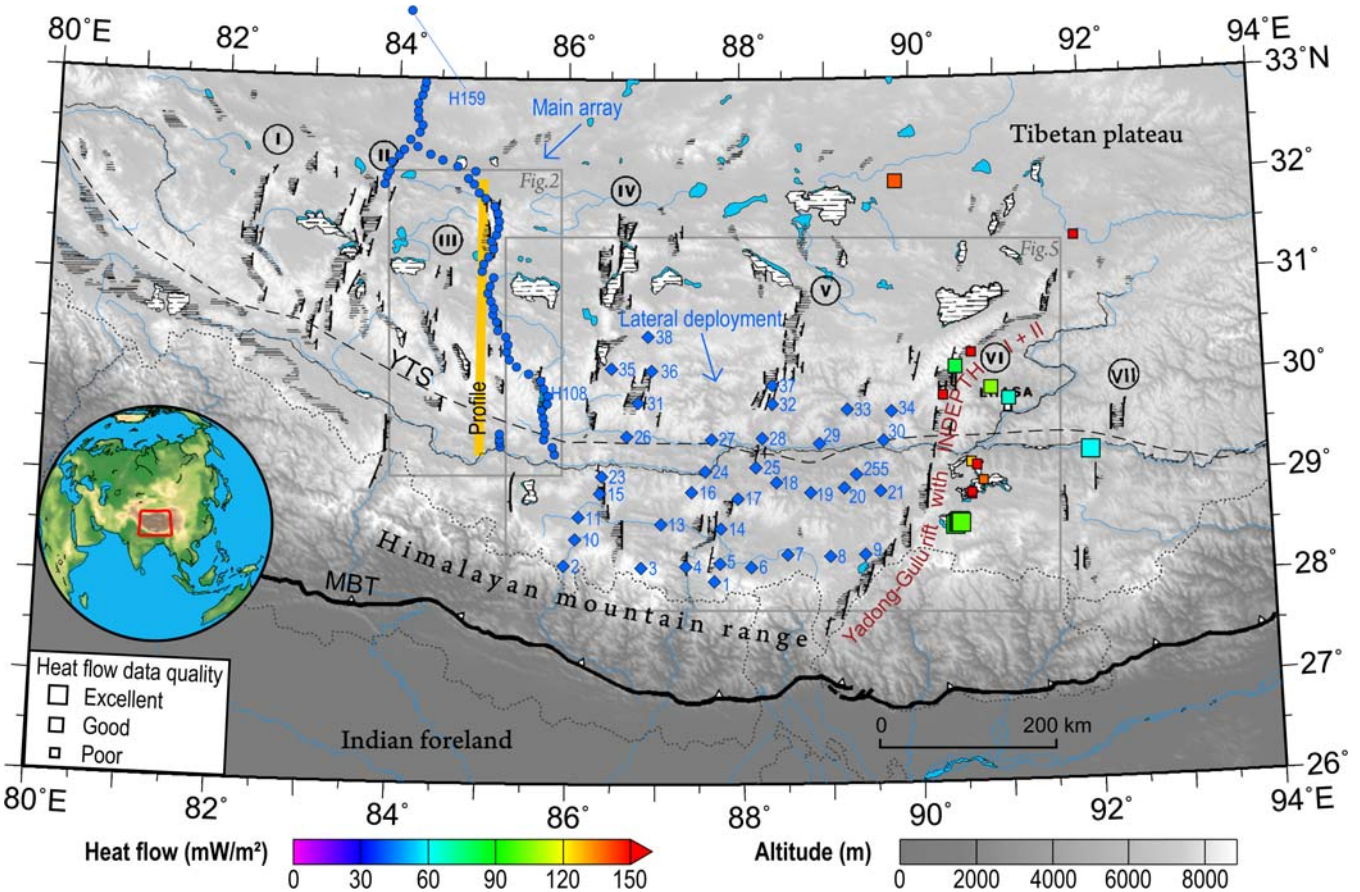

Fig. 1. Topographic map of southern Tibet, with an overlay of the original map from Armijo *et al.* (1986, 13 864, Fig. 28) in black: their map shows Quaternary normal fault traces (solid lines) bounding grabens, the associated depressions (horizontally striped areas), and lakes (horizontally striped areas with white background). Geo-referencing of the maps was performed using river and lake shapes in the central area. Roman numerals point to seven main rift systems discussed in Armijo *et al.* (1986), number VI being the Yadong-Gulu rift. Blue circles and diamonds mark broadband seismological stations from the Hi-CLIMB experiment (phase 2), from the main array and from the lateral deployment, respectively. Yellow line shows the location of the migrated profile on Figure 2. Heat flow data and quality (squares) are from Pollack *et al.* (1993). YTS, Yarlung-Tsangpo Suture. MBT, Main Boundary Thrust. The location of Figures 2 and 5 are shown for reference. Inset shows the location of this map in Asia.

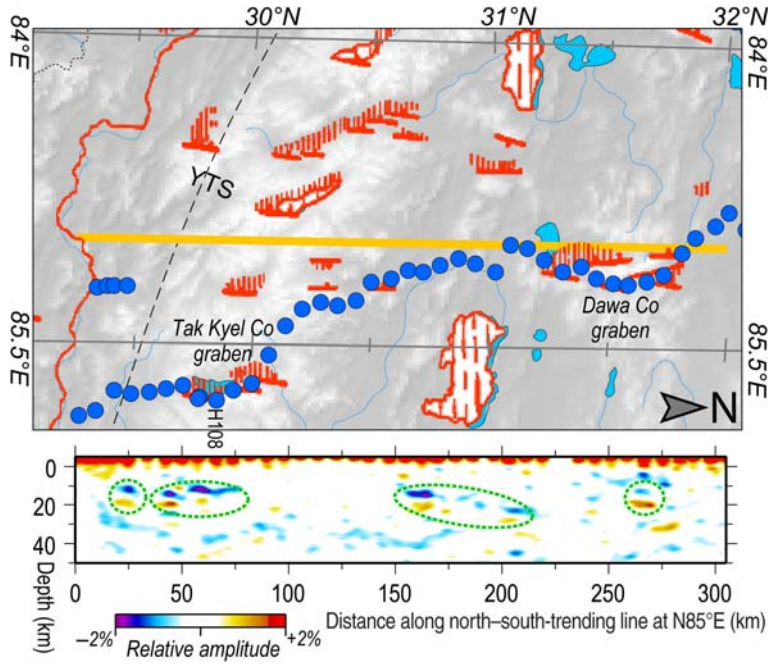

Fig. 2. Map of main array stations and projected profile, with Quaternary normal fault traces, depressions and lakes in red (see Fig. 1 for symbol explanation and location of this map). Note that the map has been rotated hence north is to the right. The profile of migrated P-to-S receiver functions (projected on to the north–south-trending yellow line at 85°E) is from the Hi-CLIMB main array (Hetényi 2007; Nábělek *et al.* 2009; Hetényi *et al.* 2010). The profile shows localized blue-over-yellow (positive-over-negative) regions that are interpreted as low-velocity zones in the upper crust (highlighted by dashed green ellipses). The blue (negative) zone beneath them is the trace of the Main Himalayan detachment (see references above). Note that the graben at station H108 (Tak Kyel Co graben) as well as the one around 31.7°N (Dawa Co graben) are located above a low-velocity zone.

background) (Brown *et al.* 1996), and strong P-to-S converted amplitudes in three-component wide-angle reflections (Makovsky *et al.* 1996). The converters that generate these unusually strong signals have been named 'bright spots'. Moreover, their location fits with the top of mid-crustal low-velocity layers deduced from the analysis of receiver functions (RF) at broad-band stations installed along the same profile (Kind *et al.* 1996). The tops of these low-velocity zones (LVZ) are usually modelled as a solid-fluid interface at *c*. 15 km depth (Makovsky *et al.* 1996). The nature of the crustal fluids is mostly given to be a granitic magma (e.g. Brown *et al.* 1996), while some suspect the presence of free aqueous fluids as well (Makovsky & Klemperer 1999). Magnetotelluric studies, performed during the INDEPTH II experiment (Chen *et al.* 1996) and during other measurements elsewhere on the plateau (Wei *et al.* 2001; Unsworth *et al.* 2005), indicate the existence of an electrically conductive zone in the southern Tibetan crust that also suggests the presence of an interconnected fluid phase. However, despite some attempts to quantitatively describe these conductive features (e.g. Li *et al.* 2003), there is no consensus on their origin (zones of partial melt or of aqueous fluid accumulation), nor on their thickness. In summary, geophysical observations show that in southern Tibet there exist zones with significant seismic P-wave velocity decrease in the upper crust (at *c*. 15 km depth) that coincide with the top of an electrically conductive zone.

The 'classical' and most extensively held interpretation of these geophysical observations is that a thick and widespread partially melted layer exists in the southern Tibetan crust (e.g. Nelson *et al.* 1996; Brown *et al.* 1996; Kind *et al.* 1996; Wei *et al.* 2001; Li *et al.* 2003; Unsworth *et al.* 2005). The view that this layer behaves as a fluid on the scale of Himalayan deformation gives strong support to a model in which the deformation of Tibet is driven by a channel-like viscous flow within the crust. This model is supported by arguments from field observations (e.g. rift flank topography in Masek *et al.* 1994) and numerical models (e.g. Royden 1996) and, since then, it

became a popular mechanism to explain the evolution of deformation of the plateau (e.g. Clark & Royden 2000; Beaumont *et al.* 2001; Shen *et al.* 2001; Jamieson *et al.* 2004; Clark *et al.* 2005). A typical set of characteristics of a channel flow model is a viscosity reduced to the $10^{17}-10^{19}$ Pa s range, a channel thickness of 15 km, and an average flow speed of 80 mm a^{-1} (Clark *et al.* 2005). Therefore, the expected seismic signature of such a feature can well be a continuous LVZ beneath the plateau with a pronounced velocity decrease on its top, as suggested by Nelson *et al.* (1996) and modelled by Hyndman & Shearer (1989).

The limitations of the INDEPTH II results and therefore of the viability of the channel flow model come from the data coverage itself. Due to the practical difficulties to perform geophysical measurements in Tibet most INDEPTH II data were collected along the Yadong-Gulu rift, which may have specific lithospheric properties. A major drawback coming from the generalization of local INDEPTH II observations is therefore that it is uncertain whether partial melt is restricted to rift-systems, such as the Yadong-Gulu rift (Fig. 1), or occurs beneath all Tibet (Yin 2005).

This study aims to assess whether regions of seismic wave velocity reduction are truly widespread across the southern Tibetan Plateau, or simply restricted to rift systems as the one where INDEPTH II data were collected. We take advantage of the Hi-CLIMB seismic experiment which includes a dense south–north profile and a lateral 2D seismic network in southern Tibet composed of stations located both in and away from individual grabens forming the rift-systems (see Fig. 1 for location and definition). First we apply passive seismic methods to assess the vertical and the horizontal extension of the LVZs in southern Tibet. Next, we compare our results to previous studies concerning the distribution and continuity of LVZs. Finally, we discuss the potential physical causes of LVZs, the relation of these to the rift systems, as well as the implications on the channel flow model and on the behaviour of the Tibetan crust.

Data processing

Seismological data used in this study have been acquired in the frame of project Hi-CLIMB. Details concerning the Hi-CLIMB experiment, including deployment and data, can be found in Hetényi (2007), Nábělek *et al.* (2009) and Hetényi *et al.* (2010). This broad-band seismology experiment was carried out to study the continental lithosphere and mountain building in the Himalaya–Tibet region. Here we focus on the second phase of the experiment, during which 113 stations were deployed for 15 months in southern and central Tibet (Fig. 1). The south–north-trending linear profile near 85°E has a station spacing of *c.* 8–10 km, which allowed us not only to image the lower part of lithosphere at high resolution, but also to have sufficient ray-path crossings at shallow depth to study the upper crust in one continuous image. The lateral deployment covers the region between this array and the former location of INDEPTH stations in the Yadong-Gulu rift (Fig. 1). Here the station spacing is sparser (*c.* 35 km in average), but the spatial distribution of the stations is better than in INDEPTH, leading to a potentially better resolution of the lateral extent of the structures at depth. Also, having some of the stations in grabens and some of them away allows the examination of the effect of grabens on the Tibetan crustal structure.

To study the structure of the crust below these stations we used receiver function analysis, a passive source method that detects waves from distant, teleseismic earthquakes that were converted from P- to S-wave on interfaces beneath the observing stations (Langston 1977). The converted waves arrive with a delay compared to the direct P-wave, and this delay is proportional to the depth of the interface where the conversion occurs, as well as to the velocity structure between the interface and the surface. The polarity of the converted P-to-S wave is positive when the impedance (product of seismic velocity and bulk density) increases with depth across the interface, and is negative when the impedance decreases. The amplitude of the converted P-to-S wave is proportional to the impedance change across the interface. Receiver functions are more suitable for detecting an eventual LVZ than active source seismology, since the illumination of structures is from below instead of above. Furthermore, the lower frequency content of RFs (typically 0.05 to *c.* 1–2 Hz) allows detection of the bottom of the LVZ as well, even when this is more likely to be a gradient than an interface. However, because of their lower frequency content, the vertical spatial resolution of the RFs will be relatively poorer.

To detect and image LVZs within the crust we apply three different methods including: migration; amplitude analysis; and waveform inversion of receiver functions.

Migration

This method is suitable when neighbouring stations are close enough to have incoming rays crossing at the depth of interest. This depth is about twice the spacing of the stations, so we apply this method to the dense linear array of stations only. The migration itself is a process that relocates the amplitude of conversions in the receiver function from time to space, and hence draws a continuous image of velocity contrasts along a profile beneath the stations. Here we use the common conversion

point method (e.g. Dueker & Sheehan 1997) and processing as detailed in Nábělek *et al.* (2009) with RFs filtered to 1 Hz maximum frequency. The resulting image is shown on Figure 2 and discussed in the next section.

Amplitude analysis

Here we take advantage of the proportionality between the amplitude of a converted wave on the RF and the impedance change across the interface that causes the conversion. Searching for LVZs, we look for the minimum amplitude of each individual RF between 1.0–2.5 s after the P-wave arrival. In case of an ordinary velocity-structure of the upper crust [$V_P = 5.8$ km s^{-1}, $V_S = 3.36$ km s^{-1} in the *iasp91* velocity-model (Kennett & Engdahl 1991)], this time range corresponds to conversions originating from interfaces between *c*. 8 and 20 km depth. Even with an eventual sedimentary cover or deviation in mean velocity that may further delay waves, we consider that this time frame is suitable to detect conversions from the upper crust. An example for a negative amplitude peak on a RF is shown on Figure 3b (left curve). This method is applied to the 2D lateral deployment, where the station spacing is too sparse to perform migration. Data selection is detailed in Appendix A.

Waveform inversion

The inversion of receiver functions aims to find a velocity–depth model that generates the synthetic RF closest in shape to the observed one in the L2-norm sense. Inversion requires good quality data and, depending on the method, considerable computation time. Here we apply two inversion approaches: a semi-linearized approach that is more likely to find local minima; and a more robust non-linear method (for details on methods and processing, see Appendix B). The semi-linear inversion was applied to all stations on data selected as described above. At stations with the more stable results, the more time consuming non-linear inversion was also performed. Two examples of RF waveforms and inversion results, showing one station with, and one without, evidence for an upper crustal LVZ (that is, a decrease and then an increase of velocity with depth) are shown on Figure 3.

The velocity–depth curves obtained by inversion are used first qualitatively and then quantitatively. The reasons for this are that the quality of the instruments and deployment sites in the lateral array was not as good as in the main array, and that the semi-linearized inversion method is not very robust. Thus we visually determine whether a LVZ in the upper crust is present or not in the velocity–depth curve obtained by inversion at each station, and identify bright spots when a V_S decrease of at least 0.5 km s^{-1} is apparent. The results of this selection are used together with the amplitude analysis, and are reported on Figure 4.

Spatial extent of low-velocity zones

The obtained migrated profile of receiver functions across the Lhasa Block is shown on Figure 2. A few localized, strongly negative anomalies dominate the

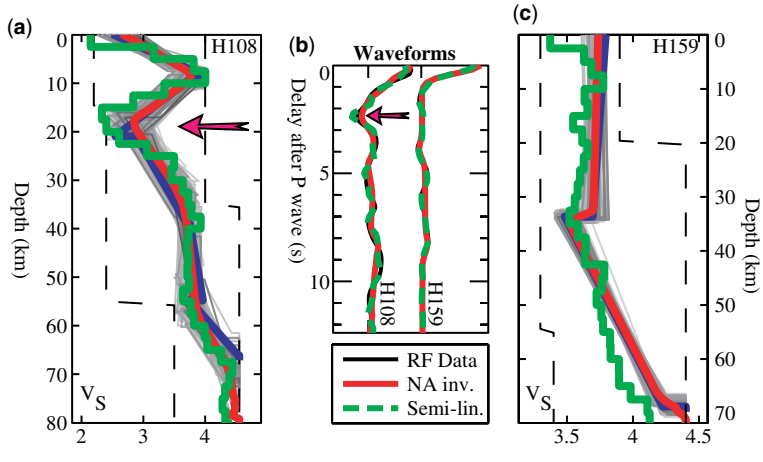

Fig. 3. Observation of low-velocity zones by receiver functions (RF) in waveforms (**b**) and velocity–depth profiles obtained by inversion (**a**, **c**). Subfigures (a) and (c) show the best model obtained by semi-linearized (green) and non-linear (NA) (blue) inversions. Grey curves show the best 100 (best 1% of all tested) models from the non-linear inversion, and red the average of these. The examples depict one station (a, H108) with (red arrow) and one station (c, H159) without an underlying low-velocity zone (see Fig. 1 for their locations, and Fig. 2 for the location of station H108 on the migrated profile). See text for more discussion and Appendix B for more details on inversion.

upper crust, which we identify as the seismic bright spots since: (1) they represent a significant drop in seismic velocity (we assume similar behaviour in V_S as in V_P); (2) they exhibit a velocity decrease with depth (negative amplitude); and (3) they are imaged in the same depth range as the bright spots seen by the INDEPTH experiment (i.e. *c*. 15 km deep). The negative anomalies are often underlain by a positive anomaly, usually of lower amplitude, and hence represent a gentler positive velocity-gradient with depth. These features form the top and bottom of LVZs. Horizontally the LVZs have a maximum length of *c*. 50 km, which might be an apparent length as the LVZs may extend beyond the aperture of the imaging rays perpendicular to the profile. One can observe that LVZs lie close to north–south grabens (Fig. 2), especially between 29.5°N and 30°N (Tak Kyel Co graben) and around 31.7°N (Dawa Co graben). There are also one or more LVZs between *c*. 30.6–31.2°N, which are not related to a graben. Other zones, for example between 30–30.6°N, have no significant velocity variations within the upper crust. The thickness determined for these three LVZs does not exceed 10 km.

To increase the spatial coverage of our study, we look at the lateral stations, where the minimum amplitudes are combined with the analysis of the inversion results (Fig. 4): an LVZ-observation is represented in darker grey. This combination shows a good correlation between the presence of LVZs and the most strongly negative amplitude anomalies. It allows the data to be split into two distinct groups (Fig. 4b). Although there is an overlap in the range of minimum amplitudes between the two sets, they form two distinct distributions. Stations where an LVZ is present possess a statistical peak at −0.050, and those where an LVZ is absent possess a peak at −0.015 (Fig. 4b).

Finally, to investigate whether the observed LVZs are laterally continuous or not, the results are reported in map-view (Fig. 5). The main and most striking observation is that there is no continuous pattern in the distribution of LVZs. Thus independently from their physical cause, they do not form a coherent sheet or continuum beneath southern Tibet.

By comparing the distribution of LVZs with that of extensional grabens, it can be argued that the loci of grabens are partly controlled by the presence of LVZs. A majority but not all (7 out of 9) stations located in individual grabens see an underlying LVZ. However, 3 out of 5 stations lying in the axis of main rift-systems but outside of mapped grabens (outlined in Armijo *et al.* 1986) are not underlain by an LVZ, showing that LVZs do not form a continuous feature along-strike of the rift-systems. There are LVZ observations outside of rift-systems (see next section), but 8 out of 13 stations located here have a regular velocity structure beneath them with no underlying LVZ.

These observations can be interpreted together with the INDEPTH experiment: (1) stations located

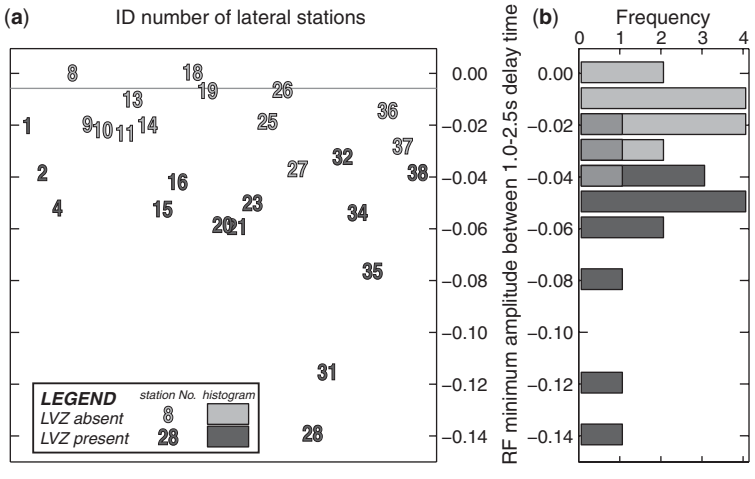

Fig. 4. Distribution of minimum amplitudes of receiver functions from lateral stations (see blue diamonds on Fig. 1 for locations) within the 1.0–2.5 s delay time range. This time window after the P-wave arrival is expected to detect upper-crustal velocity variations. LVZs seen by RF inversions are reported in colour code: observation of LVZ in dark grey shows correlation with more negative amplitudes, and their absence in light grey shows correlation with the less negative amplitudes. Numbers corresponding to stations with usable three-component data are reported one after another (**a**). The histogram (**b**) shows that the distribution of these amplitudes is non Gaussian, and corresponds to one group of stations without and one group with observed upper crustal LVZs.

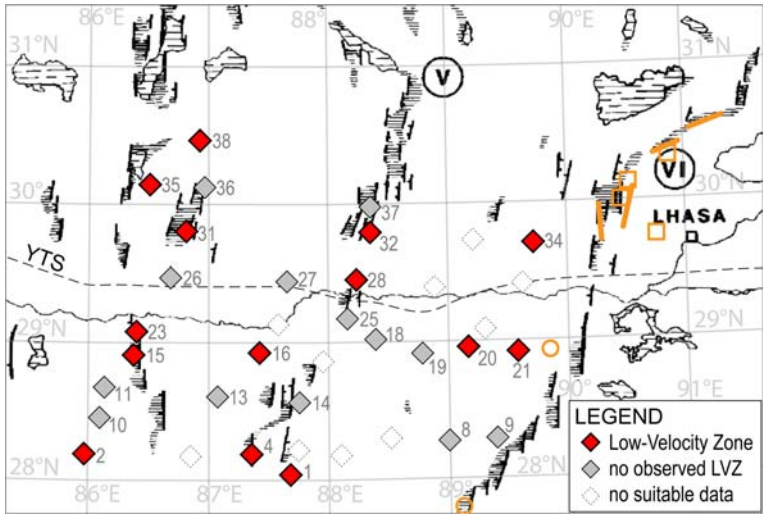

Fig. 5. Low-velocity zone observations in southern Tibet. Earlier observations based on INDEPTH II data are shown in orange: lines (Makovsky *et al.* 1999), squares (Yuan *et al.* 1997), and circles (Mitra *et al.* 2005). Stations from the lateral deployment of the Hi-CLIMB experiment (diamonds) are reported with a colour code indicating whether an LVZ is observed or not. Rift systems, grabens and associated depressions, as well as lakes are from Armijo *et al.* (1986) (see Fig. 1 for symbol definition). See text for discussion and interpretation. Stations in grabens: 1, 4, 15, 23, 31, 32, 35, 36, 37. Stations in rift-systems but outside grabens: 14, 25, 26, 28, 38. Stations outside of rift-systems: 2, 8, 9, 10, 11, 13, 16, 18, 19, 20, 21, 27, 34.

in grabens are likely to detect underlying LVZs; (2) the additional spatial coverage given by the Hi-CLIMB lateral stations shows that LVZs are localized; and (3) at the scale of the study area, $400 \times 200\ km^2$, LVZs do not form a continuous crustal feature. Therefore it is more plausible that there is no generalized physical process in the crust, such as widespread partial melt. This is also supported by the observation that the average crustal V_P/V_S ratio throughout the sampled area in Tibet (Hetényi 2007; Nábělek *et al.* 2009; Hetényi *et al.* 2010) shows values close to the worldwide average for continental areas (Zandt & Ammon 1995), and not high values expected for large amounts of partial melt (Watanabe 1993).

Potential nature of the fluids and the viability of channel flow

The question of what causes the LVZs observed in Tibet and what are the respective amounts and roles of magmatic and aqueous fluids has been broadly discussed in the literature (e.g. Makovsky & Klemperer 1999; Li *et al.* 2003).

Makovsky & Klemperer (1999) demonstrated that the observed INDEPTH II bright spot reflections are likely to be generated by 10% volume of free aqueous fluids in the Tibetan middle crust. One can infer that these free aqueous fluids may come from metamorphic dehydration reactions at depth. A regional contribution from below the LVZs may be derived from underplating of the Indian lower crust and its eclogitization liberating fluids at depth around the Yarlung-Tsangpo suture and further north beneath the Lhasa block (Hetényi *et al.* 2007). If the free fluids are not all driven away by the overlying Main Himalayan thrust, they can migrate upwards toward the LVZs. Free aqueous fluids may also come from above, as infiltrations of meteoric waters along graben-bounding normal faults. Whatever the scenario, these aqueous fluids do not preclude the existence of magmatic fluids and may even help to initiate or to further enhance localized melting. However, for most authors, this process is a trivial addition to models dominated by the presence of magmatic fluids (e.g. Nelson *et al.* 1996). Although it has not been unequivocally demonstrated, the presence of magma bodies within the Tibetan crust coinciding with the LVZs is suggested, given the locally high heat flow and young volcanism at surface (e.g. Brown *et al.* 1996). In this study, we argue against thick and widespread partial melt; in the meantime, given the thickness of the crust (*c.* 80 km) and the thickness of the LVZs (*c.* 10 km), the possibility of having thin layers of molten rock in the crust with high V_P/V_S ratio cannot be ruled out. A quantitative characterization of the LVZs seems feasible by joint application of P-to-S and S-to-P receiver

functions (Wittlinger *et al.* 2009) yielding an independent estimate for V_P/V_S ratio of the LVZs that would be characteristic of either aqueous or magmatic fluids (Watanabe 1993). This method at present implies potentially large errors due to the thinness of the LVZs, and is not in the scope of our study.

The origin of aqueous fluids that enhance or initiate local partial melt within the crust can be speculated from our results and Figure 5. There are 4 stations in 4 grabens that do not detect an underlying LVZ (stations 14, 25, 36, 37), but in all of these grabens there is another station beneath which an LVZ can be observed (respectively stations 1, 28, 31, 32). This distribution is non-conclusive: it can either mean localized melting at depth followed by rifting initiation and rapid propagation away at surface, or a tectonic event followed by fluid circulation and localized partial melting. However, there are 5 stations in areas where no grabens have been previously mapped that detect an underlying LVZ (stations 2, 16, 20, 21 and 34): this favours a thermally driven rifting in southern Tibet.

Summarizing our results from the channel flow perspective, our images show seismic LVZs that are of comparable thickness that channels in crustal flow models (*c*. 10 km scale). The cause of these LVZs can still be both aqueous fluids and partial melt: a 10-km thick layer with a few percent partial melt embedded in an 80-km thick crust does not significantly raise the average V_P/V_S-ratio. In the meantime, what is clearly shown by the spatial distribution of LVZ observations is that a continuous sheet of partial melt beneath Tibet is highly implausible. Therefore the mechanical viability of the channel flow model as a governing force of the plateau's general deformation is strongly questioned. Instead, both LVZs and rifting appear to be localized zones of weakness that help to maintain Tibet's deformation broad on the crustal scale, and potentially contribute to the difficulty in distinguishing between block and continuum deformation models on the large scale.

Conclusions

We have focused on the spatial distribution of LVZs in southern Tibet using new seismological data and various analyses of receiver functions. Our study has shown that these LVZs are limited to 10 km in thickness, and that they do not form a continuous layer beneath the plateau. Indeed, these LVZs occur mostly in and also away from extensional grabens, without any evident and common connectivity pattern. These results, as well as normal average crustal V_P/V_S-ratios, question the thick and widespread partial melt scenario that was suggested to characterize the southern Tibetan crust, and which is the major pillar of channel flow models.

Our study has pointed out the importance of denser spatial sampling of geophysical data. At the present stage of data coverage in Tibet, acquiring new heat-flow data, both in and away from grabens, would be of invaluable help to build a comprehensive picture of the thermal state of the lithosphere, and therefore of the geodynamics and growth of Tibet.

We are grateful to the numerous people have who contributed to the data acquisition in the field, and to John Nábělek for the seismology data. Many thanks to Richard Gloaguen and Lothar Ratschbacher for promptly editing this volume. We warmly thank the constructive criticism of reviewers Ian Watkinson and Michele Zucali, including the most thorough grammatical corrections we have ever seen in a review. Maps were generated with the Generic Mapping Tool (Wessel & Smith 1991). Feedback from several people following an ETH-seminar and a 2009 EGU-talk helped to focus the conclusions. This work was supported by Swiss National Science Foundation grant 200020-107889.

Appendix A

Data selection for RF amplitude analysis and inversion

Receiver functions were calculated as indicated in Nábělek *et al.* (2009) but with 2 Hz maximum frequency content. First an automatic, then a visual selection process was applied to keep the best quality traces at each station. The criteria included: (1) selection of $M \geq 6.4$ events in the epicentral distance range of 30–95°; (2) exclusion of numerous small aftershocks closely following large magnitude events; (3) exclusion of traces based on signal-to-noise ratio of the original three-component data; and (4) automatic examination of the receiver function shape based on the time of its peak amplitude. As a result, 123 traces (between 1 and 16 at each station) were kept at the 27 lateral stations, and stacked for amplitude analysis. Further 10 stations of the lateral deployment did not produce good quality data in the analysed frequency band.

Appendix B

Inversion methods and details

Semi-linearized inversion (Ammon *et al.* 1990) tries a limited number of velocity models by modifying one or more initial models, the choice of which is crucial to the success of the inversion. The depth range to be modelled is divided into depth-slices of fixed thickness and constant velocity. The V_P/V_S ratio is fixed, which is a simplifying

assumption, but effectively reduces the number of parameters to invert, and hence calculation costs. Thus the only parameter to recover is the shear-wave velocity in each layer.

In order to stabilize the semi-linear inversions, a step-like resolution procedure was followed, starting from low frequencies (0.05 Hz) and thick layers (10 km), and ending with high frequencies (0.5 Hz) and thin layers (2.5 km). At each step, either the frequency was increased or the thickness was decreased. Finally, the highest frequency solution was low-pass filtered and compared to the RF filtered similarly, which allowed an estimate of the robustness of the procedure. The final high-frequency results are step-like velocity–depth curves, such as the ones in green on Figure 3. The drawback of this method is (1) the use of constant V_P/V_S ratio, which could imply an error on the shape of the velocity-structure, and (2) the strong dependency on the initially assumed model. However, as the average crustal V_P/V_S-ratio is in the regular range (Hetényi 2007; Nábělek *et al.* 2009; Hetényi *et al.* 2010) this error is considered to be minor.

For the non-linear (stochastic) inversion scheme, the Neighbourhood Algorithm (NA) was applied (Sambridge 1999). This technique has the advantage of: (1) varying both V_P and V_S, as well as the thickness of the layers; and (2) performing a more complete search in the parameter space, that in general helps to avoid falling in local minima. The number of layers has to be fixed in advance, and the range of variation for each parameter to invert has to be bound as well. It also allows the presence of velocity-gradients. The cost for these advantages is increased computation time compared to the semi-linearized approach.

In our study, the initial model was taken from the semi-linear inversion result, and the V_P/V_S ratio was allowed to vary between 1.70–1.90. The inversions have been run using 100 iterations with 100 velocity-models in each (a total of 10 000 models) to reproduce traces filtered up to 0.5 Hz. In the final results, the best 100 (best 1% of all tested) velocity-models (in grey), their average (red), and the best model (blue) are shown (Fig. 3).

The velocity-models resulting from the inversions were not always similar between low and high frequencies, and/or between the semi-linearized scheme and the NA. Only at least partially coherent results were used for the interpretation concerning the velocity-structure, and hence the presence of low-velocity zones.

References

Ammon, C. J., Randall, G. E. & Zandt, G. 1990. On the non-uniqueness of receiver function inversions. *Journal of Geophysical Research*, **95**, 15 303–15 318.

Armijo, R., Tapponnier, P., Mercier, J. L. & Han, T. L. 1986. Quaternary extension in southern Tibet: field observations and tectonic implications. *Journal of Geophysical Research*, **91**, 13803–13872.

Avouac, J.-P. & Tapponnier, P. 1993. Kinematic model of active deformation in Central Asia. *Geophysics Research Letters*, **20**, 895–898.

Beaumont, C., Jamieson, R. A., Nguyen, M. H. & Lee, B. 2001. Himalayan tectonics explained by extrusion of a low-viscosity crustal channel coupled to focused surface denudation. *Nature*, **414**, 738–742.

Brown, L. D., Zhao, W. J. *et al.* 1996. Bright spots, structure, and magmatism in southern Tibet from INDEPTH seismic reflection profiling. *Science*, **274**, 1688–1690.

Chen, L., Booker, J. R., Jones, A. G., Wu, N., Unsworth, M. J., Wei, W. & Tan, H. 1996. Electrically conductive crust in Southern Tibet from INDEPTH magnetotelluric surveying. *Science*, **274**, 1694–1695.

Clark, M. K. & Royden, L. H. 2000. Topographic ooze: building of Tibet by lower crustal flow. *Geology*, **28**, 703–706.

Clark, M. K., Bush, J. W. M. & Royden, L. H. 2005. Dynamic topography produced by lower crustal flow against rheological strength heterogeneities bordering the Tibetan Plateau. *Geophysical Journal International*, **162**, 575–590.

Dueker, K. & Sheehan, A. 1997. Mantle discontinuity structure from midpoint stacks of converted P to S waves across the Yellowstone hotspot track. *Journal of Geophysical Research*, **102**, 8313–8327.

England, P. & Molnar, P. 1997. Active deformation of Asia: from kinematics to dynamics. *Science*, **278**, 647–650.

Haines, S. S., Klemperer, S. L. *et al.* 2003. INDEPTH III seismic data: from surface observations to deep crustal processes in Tibet. *Tectonics*, **22**, 1001, doi: 10.1029/2001TC001305, 2003.

Hetényi, G. 2007. *Evolution of deformation of the Himalayan prism: from imaging to modelling*. PhD thesis, École Normale Supérieure, Université Paris-Sud XI.

Hetényi, G., Cattin, R., Brunet, F., Vergne, J., Bollinger, L., Nábělek, J. L. & Diament, M. 2007. Density distribution of the India plate beneath the Tibetan Plateau: geophysical and petrological constraints on the kinetics of lower-crustal eclogitization. *Earth and Planetary Science Letters*, **264**, 226–244, doi: 10.1016/j.epsl.2007.09.036.

Hetényi, G., Cattin, R. & Vergne, J. 2010. *Geodynamics of Tibet and the Himalayas – Geophysical advances from imaging and modelling*. LAP Lambert Academy Publisher, Saarbrucken. ISBN 978-3-8383-2353-4, 1–408.

Houseman, G. & England, P. 1993. Crustal thickening v. lateral expulsion in the Indian–Asian continental collision. *Journal of Geophysical Research*, **98**, 12233–12249.

Hyndman, R. D. & Shearer, P. M. 1989. Water in the lower continental-crust: modeling magnetotelluric and seismic-reflection results. *Geophysical Journal International*, **98**, 343–365.

Jamieson, R. A., Beaumont, C., Medvedev, S. & Nguyen, M. H. 2004. Crustal channel flows: 2. Numerical models with implications for metamorphism in the Himalayan–Tibetan orogen. *Journal of Geophysical Research*, **109**, B06407.

KENNETT, B. L. N. & ENGDAHL, E. R. 1991. Traveltimes for global earthquake location and phase identification. *Geophysical Journal International*, **105**, 429–465.

KIND, R., NI, J. *ET AL.* 1996. Evidence from earthquake data for partially molten crustal layer in southern Tibet. *Science*, **274**, 1692–1694.

LANGSTON, C. 1977. Corvallis, oregon, crustal and upper mantle receiver structure from teleseismic P-waves and S-waves. *Bulletin of the Seismological Society of America*, **67**, 713–724.

LI, S. H., UNSWORTH, M. J., BOOKER, J. R., WEI, W. B., TAN, H. D. & JONES, A. G. 2003. Partial melt or aqueous fluid in the mid-crust of southern Tibet? Constraints from INDEPTH magnetotelluric data. *Geophysical Journal International*, **153**, 289–304.

MAKOVSKY, Y. & KLEMPERER, S. L. 1999. Measuring the seismic properties of the Tibetan bright spots: evidence for free aqueous fluids in the Tibetan middle crust. *Journal of Geophysical Research*, **104**, 10795–10825.

MAKOVSKY, Y., KLEMPERER, S. L., RATSCHBACHER, L., BROWN, L. D., LI, M., ZHAO, W. J. & MENG, F. L. 1996. INDEPTH wide-angle reflection observation of P-wave-to-S-wave conversion from crustal bright spots in Tibet. *Science*, **274**, 1690–1691.

MASEK, J. G., ISACKS, B. L., GUBBELS, T. L., FIELDING, E. J. & BROWAEYS, J. 1994. Erosion and tectonics at the margins of continental plateaus. *Journal of Geophysical Research*, **99**, 13941–13956.

MITRA, S., PRIESTLEY, K., BHATTACHARYYA, A. K. & GAUR, V. K. 2005. Crustal structure and earthquake focal depths beneath northeastern India and southern Tibet. *Geophysical Journal International*, **160**, 227–248.

MOLNAR, P. & STOCK, J. M. 2009. Slowing of India's convergence with Eurasia since 20 Ma and its implications for Tibetan mantle dynamics. *Tectonics*, **28**, TC3001, doi: 10.1029/2008TC002271.

MOLNAR, P. & TAPPONNIER, P. 1975. Cenozoic tectonics of Asia – effects of a continental collision. *Science*, **189**, 419–426.

MOLNAR, P., FITCH, T. J. & WU, F. T. 1973. Fault plane solutions of shallow earthquakes and contemporary tectonics in Asia. *Earth and Planetary Science Letters*, **19**, 101–112.

NÁBĚLEK, J., HETÉNYI, G. *ET AL.* & THE HI-CLIMB TEAM 2009. Underplating in the Himalaya-Tibet collision zone revealed by the Hi-CLIMB experiment. *Science*, **325**, 1371–1374, doi: 10.1126/science.1167719.

NELSON, K. D., ZHAO, W. J. *ET AL.* 1996. Partially molten middle crust beneath southern Tibet: synthesis of project INDEPTH results. *Science*, **274**, 1684–1688.

PATRIAT, P. & ACHACHE, J. 1984. India–Eurasia collision chronology has implications for crustal shortening and driving mechanism of plates. *Nature*, **311**, 615–621.

POLLACK, H. N., HURTER, S. J. & JOHNSON, J. R. 1993. Heat flow from the Earth's interior: analysis of the global data set. *Reviews of Geophysics*, **31**, 267–280.

ROYDEN, L. 1996. Coupling and decoupling of crust and mantle in convergent orogens: implications for strain partitioning in the crust. *Journal of Geophysical Research*, **101**, 17679–17705.

SAMBRIDGE, M. 1999. Geophysical inversion with a neighbourhood algorithm – I. Searching a parameter space. *Geophysical Journal International*, **138**, 479–494.

SHEN, F., ROYDEN, L. H. & BURCHFIEL, B. C. 2001. Large-scale crustal deformation of the Tibetan Plateau. *Journal of Geophysical Research*, **106**, 6793–6816.

THATCHER, W. 2007. Microplate model for the present-day deformation of Tibet. *Journal of Geophysical Research*, **112**, B01401, doi: 10.1029/2005JB004244.

UNSWORTH, M. J., JONES, A. G., WEI, W., MARQUIS, G., GOKARN, S. G. & SPRATT, J. E. 2005. Crustal rheology of the Himalaya and southern Tibet inferred from magnetotelluric data. *Nature*, **438**, 78–81.

WATANABE, T. 1993. Effects of water and melt on seismic velocities and their application to characterization of seismic reflectors. *Geophysical Research Letters*, **20**, 2933–2936.

WEI, W. B., UNSWORTH, M. *ET AL.* 2001. Detection of widespread fluids in the Tibetan crust by magnetotelluric studies. *Science*, **292**, 716–718.

WESSEL, P. & SMITH, W. 1991. Free software helps map and display data. *EoS Transactions American Geophysical Union*, **72**, 441 and 445–446.

WITTLINGER, G., FARRA, V., HETÉNYI, G., VERGNE, J. & NÁBĚLEK, J. 2009. Seismic velocities in Southern Tibet lower crust. A receiver function approach for eclogite detection. *Geophysical Journal International*, **177**, 1037–1049, doi: 10.1111/j.1365-246X.2008.04084.x.

YIN, A. 2005. Cenozoic tectonic evolution of the Himalayan orogen as constrained by along-strike variation of structural geometry, exhumation history, and foreland sedimentation. *Earth-Science Reviews*, **76**, 1–131.

YUAN, X., NI, J., KIND, R., MECHIE, J. & SANDVOL, E. 1997. Lithospheric and upper mantle structure of southern Tibet from a seismological passive source experiment. *Journal of Geophysical Research*, **102**, 27491–27500.

ZANDT, G. & AMMON, C. J. 1995. Continental crust composition constrained by measurements of crustal Poisson's ration. *Nature*, **374**, 152–154.

ZHANG, P. Z., SHEN, Z., WANG, M., GAN, W. J., BURGMANN, R. & MOLNAR, P. 2004. Continuous deformation of the Tibetan Plateau from global positioning system data. *Geology*, **32**, 809–812.

ZHAO, W. J., NELSON, K. D. & PROJECT INDEPTH TEAM. 1993. Deep seismic-reflection evidence for continental underthrusting beneath southern Tibet. *Nature*, **366**, 557–559.